

## Original article

# Parameters optimization of storage capacity of hole-bottom freezing sampling technique for natural gas hydrates

Jiang Lei<sup>1,2</sup>, Wei Guo<sup>1,2</sup>\*, Xiang Yang<sup>2</sup>, Pengyu Zhang<sup>1,2</sup>, Rui Jia<sup>1,2</sup>, Yuan Wang<sup>1,2</sup>\*

<sup>1</sup>College of Construction Engineering, Jilin University, Changchun 130021, P. R. China

<sup>2</sup>Key Lab of Ministry of Natural Resources for Drilling and Exploitation Technology in Complex Conditions, Jilin University, Changchun 130021, P. R. China

### Keywords:

Natural gas hydrate  
freezing sampling technology  
coolant  
phase change heat transfer  
storage efficiency

### Cited as:

Lei, J., Guo, W., Yang, X., Zhang, P., Jia, R., Wang, Y. Parameters optimization of storage capacity of hole-bottom freezing sampling technique for natural gas hydrates. *Advances in Geo-Energy Research*, 2024, 12(1): 66-76.  
<https://doi.org/10.46690/ager.2024.04.06>

### Abstract:

The coolant must be pre-stored in the sampler before the freezing procedure for natural gas hydrate sampling is applied. The coolant's storage capacity throughout the sampler-lowering procedure is crucial to ensure successful sampling. In this study, the key factors influencing storage capacity were coolant density, dry ice specific surface area, ambient pressure, and temperature difference. An orthogonal method was used to analyze each factor's level of influence and potential action processes. The results indicated that ambient pressure, specific surface area, coolant density, and temperature difference all had significant impact. Ambient pressure affects the phase-change path of dry ice, and high pressure increases the likelihood of dry ice melting, greatly reducing latent heat. The larger specific surface area could help to generate a compact dry ice layer to protect the interior, but it may cause cold energy loss during the freezing process. Dry ice, with a smaller specific surface area, may be a better option. Low-temperature alcohol can separate the dry ice layer from the surrounding environment, allowing for heat exchange. However, a low coolant density may promote heat exchange between the alcohol layer and surrounding environment, resulting in the loss of dry ice. The appropriate coolant formulation comprised of a mixture of 2.5 kg of granular dry ice and 1 L of alcohol, temperature difference maintained at 105 K, and the working pressure of 0.1 MPa.

## 1. Introduction

With the scarcity of conventional oil and gas resources, the exploration and exploitation of unconventional oil and gas resources is becoming increasingly important, which is critical to national energy security (Lu et al., 2019; Xia et al., 2023). Natural gas hydrates, along with other unconventional reservoirs, such as shale gas (Middleton et al., 2017; Zhao et al., 2023), coalbed methane gas (Xue et al., 2022; Zou et al., 2022), and oil shale (Kang et al., 2020) are seen as valuable alternative resources (Zhang et al., 2022a). Simultaneously, to reduce greenhouse gas emissions, the mining of hydrates via the replacement method to accomplish geological carbon dioxide (CO<sub>2</sub>) storage is also considered as solutions (Ali et al., 2022; Zhang et al., 2024). Hence, the exploration and production of natural gas hydrates have garnered global

attention (Zhu et al., 2023; Wang et al., 2024). The hydrate sampling technique is the most direct exploration method, with applications including hydrate physical property analysis, resource potential assessment, sweet spots, and carbon storage site assessment.

It is critical to get insitu cores of hydrate sediments because they are metastable substances. Pressure-preservation sampling technology is a conventional method for obtaining hydrate cores (Wang et al., 2022; Guo et al., 2023), with typical samplers including pressure core barrels, pressure core samplers, and pressure temperature core sampler (Ryu et al., 2013; Kumar et al., 2014; Stern and Lorenson, 2014; Inada and Yamamoto, 2015). However, it has been observed that the overall success rate of existing pressure-preservation samplers is low, owing primarily to the seal failure of the ball or flap valves in the complex sampling environment (Schultheiss et

al., 2009; Riedel et al., 2010; Yamamoto et al., 2014). Despite this, pressure-preservation sampling technology remains as one of the most feasible methods for overcoming the problem of hydrate decomposition induced by pressure changes during the sampling process.

Natural gas hydrates remain stable under suitable temperature and pressure conditions, forming a phase equilibrium curve. The phase equilibrium curve of the methane hydrate was calculated according to Colorado School of Mines Hydrate Kinetics model (Tsuji et al., 2005; Sloan Jr et al., 2007; Babakhani et al., 2015; Xiao et al., 2020), as shown in Fig. 1. The decomposition pressure is 0.1 MPa at 190 K, indicating that the produced hydrate cores remain stable. The phase equilibrium property of hydrates at low temperatures provides a theoretical basis for the freeze sampling technique, but it requires higher accuracy. Fortunately, the unique self-preservation effect of hydrates allows this. The self-preservation effect refers to the property in which hydrates have an anomalously low decomposition rate between 242 and 272 K when the decomposition pressure is atmospheric (Stern et al., 2001; Falenty et al., 2014). Previous studies have indicated that the hydrate decomposes by only 0.85% in 10 days at a temperature of 255 K (Gudmundsson et al., 1994). To achieve sample requirements, only the hydrate cores in the self-preservation zone needed to be frozen. Furthermore, clay silt hydrate exhibited a high self-preservation effect between 243 and 253 K (Zhang et al., 2022b), establishing a theoretical basis for its application in marine hydrate sampling.

Based on the abovementioned principles, Jilin University proposed a hole-bottom freeze-sampling technique and conducted sampler design (Sun et al., 2015), refrigeration media (Sun et al., 2018; Wang et al., 2020), freezing efficiency optimization (Guo et al., 2021), and sampler application (Guo et al., 2020) to demonstrate the technique's feasibility for sampling of marine clay silt hydrates. The most recent type is the double-latch wire-line hole-bottom freezing sampler (HBFS), the working of which is shown in Fig. 2. First, the HBFS was debugged abroad the drill ship by packing coolant and testing the sampler's operational reliability (Fig. 2(a)). The sampler was then lowered from the interior of the outer pipe to the hole's button (Fig. 2(b)). When the hydrate layer was sampled, the coolant was injected from the storage chamber to the freezing chamber by adjusting the control mechanism causing the temperature of the hydrate cores to rapidly decrease to the desired level (Fig. 2(c)). Finally, the HBFS was recovered to the drillship's deck (Fig. 2(d)). To achieve the best freezing efficiency, the HBFS uses a mixture of dry ice and alcohol as the coolant and obtains the formula for best freezing efficiency (Guo et al., 2021).

The current efforts are mostly concerned with the sampler's functional testing and the temperatures of the frozen cores, which typically demand an excessive amount of coolant. Hydrate reservoirs in the South China Sea are typically located at water depths of 900-1,500 m and 300 m below the seafloor (Kong et al., 2018; Li et al., 2018; Ye et al., 2020), implying that it would take a long time to lower samplers to be lowered from the drillship to the bottom of the hole. It should be noted that coolant was contained within the sampler. The coolant's

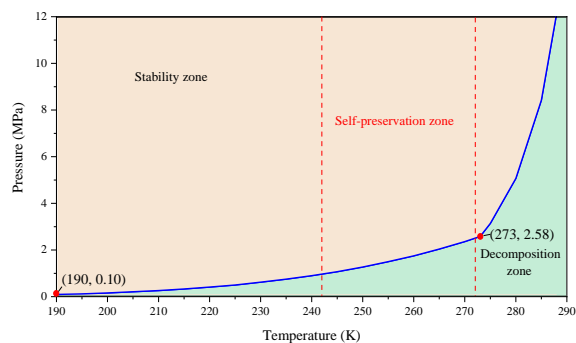


**Fig. 1.** Phase equilibrium and self-preservation effect of methane hydrates.

storage capacity is critical, as it determines whether there will be sufficient cold energy for the rapid freezing of hydrate cores after sampling, ensures that the temperature of frozen cores does not fluctuate during recovery, and is related to the freezing sampling technique's success. However, the coolant changes throughout this process were not thoroughly considered.

This study improves an indoor experimental apparatus based on the HBFS and uses the orthogonal method to study the effects of coolant density, dry ice specific surface area, ambient pressure and temperature difference on the coolant storage capacity. The storage efficiency and exergy of the coolant during storage process are analyzed and correlations are considered. Finally, optimized formulation parameters are obtained, which are useful for the coolant storage and subsequent injection. This study provides a theoretical basis for optimizing the hole-bottom freezing technique for gas hydrate sampling.

## 2. Experimental methods

### 2.1 Orthogonal experimental design

The orthogonal method is a mathematical statistical method that uses orthogonal tables to arrange and analyze multi-factor experiments. Its core is to replace comprehensive experiments with a few experiments, which can effectively reduce the number of experiments and improve efficiency, and at the same time obtain representative experimental conditions. This method is widely used in industrial and scientific research fields for program optimization. The coolant density (CD), dry ice specific surface area (SA), ambient pressure (AP) and temperature difference (TD) were identified as have essential effects after examining the coolant's preparation technique and storage conditions.

- 1) CD was defined as the mass of dry ice per unit volume of coolant, which could affect the energy density of the coolant and was controlled by adjusting the volume of alcohol, as shown in Fig. 3(a).
- 2) SA was controlled by changing the shape of the dry ice and could affect the heat exchange area between the dry ice and the external environment, as shown in Fig. 3(b).
- 3) AP transformed the phase change process of dry ice, as shown in Fig. 3(c).

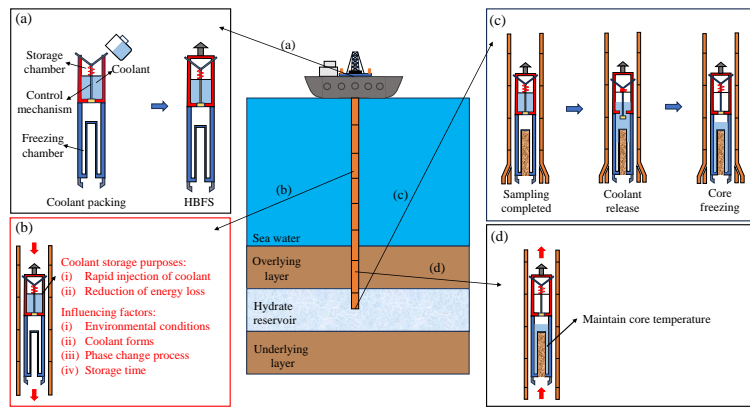


**Fig. 2.** The working process of HBFS: (a) debugging, (b) lowering, (c) sampling, and (d) recovery.

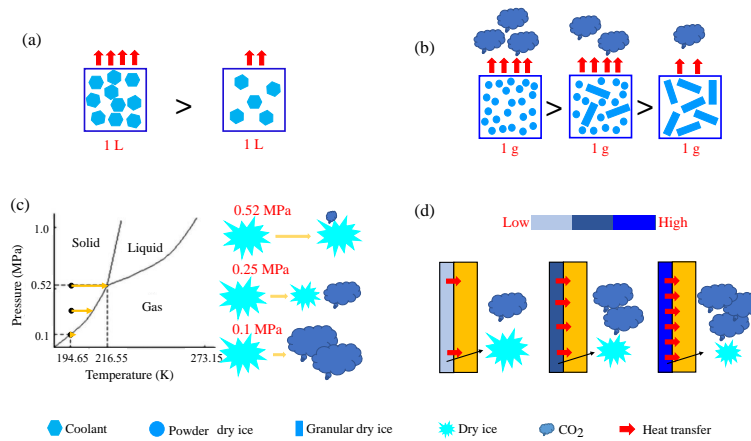


**Fig. 3.** Schematic of the influence principle of different factors: (a) coolant density, (b) specific surface area, (c) ambient pressure, and (d) temperature difference.

- 4) TD affects the heat exchange rate between the coolant and environment, as shown in Fig. 3(d).

Therefore, the following experimental conditions were established to satisfy the energy required to freeze the hydrate cores, as shown in Tables 1 and 2:

## 2.2 Experimental apparatus

The experimental apparatus used was identical to the storage mechanism used in our previous study (Guo et al., 2021), as shown in Fig. 4(a). The structural parameters of the storage chamber are listed in Table 3. A customized long-term temperature sensor with four monitoring points was installed in the storage chamber with an accuracy of 0.2% FS and a temperature range of 123–423 K.  $TS_1$  was used to monitor the gas temperature, while  $TS_2$ ,  $TS_3$ , and  $TS_4$  were used to monitor the coolant temperature. The positional parameters are presented in Fig. 4(b). A pressure sensor was used to monitor the pressure inside the storage chamber with an accuracy of 0.25% FS and a range of 20 MPa. A back pressure valve was used to regulate the  $CO_2$  release pressure. A paperless recorder was used to record the experimental data at a recording interval of 1 s.

**Table 1.** Factor level table for coolant storage.

Levels	CD (dry ice, kg; alcohol, L)	SA (powder, kg; granular, kg)	AP (MPa)	TD (K)
1	2.5; 1.5	2.5; 0	0.1	120
2	2.5; 1.75	1.25; 1.25	0.2	115
3	2.5; 1.25	1.67; 0.83	0.4	110
4	2.5; 1.0	0; 2.5	non-exhaust	105

## 2.3 Experimental materials

This study included three main experimental materials: dry ice, alcohol, and liquid nitrogen. Dry ice was primarily used as a phase-change refrigerant to quickly chill the hydrate cores. Two types of dry ice—powder and granular—were used in the experiments. Alcohol was used as a catalyst, and dry ice carrier was used to control the volume, viscosity, and energy density of the coolant. Liquid nitrogen was used to regulate the initial coolant temperature.

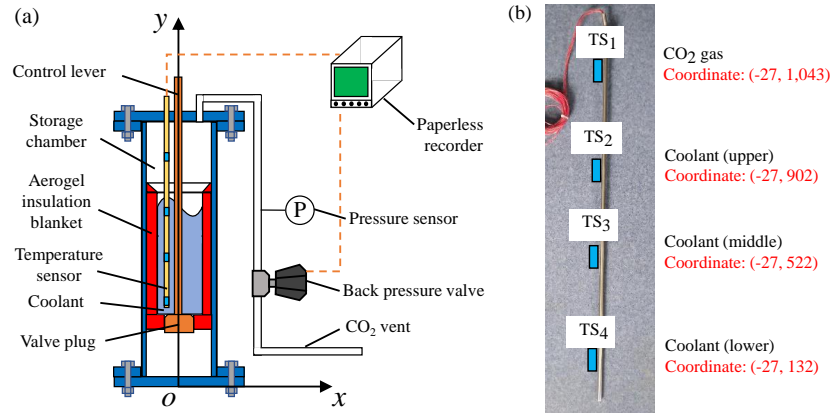


**Fig. 4.** Experimental apparatus: (a) schematic and (b) temperature sensor.

**Table 2.** Orthogonal experimental program.

No.	CD	SA	AP	TD
1	CD1	SA1	AP1	TD1
2	CD2	SA1	AP2	TD2
3	CD3	SA1	AP3	TD3
4	CD4	SA1	AP4	TD4
5	CD3	SA2	AP1	TD2
6	CD4	SA2	AP2	TD1
7	CD1	SA2	AP3	TD4
8	CD2	SA2	AP4	TD3
9	CD4	SA3	AP1	TD3
10	CD3	SA3	AP2	TD4
11	CD2	SA3	AP3	TD1
12	CD1	SA3	AP4	TD2
13	CD2	SA4	AP1	TD4
14	CD1	SA4	AP2	TD3
15	CD4	SA4	AP3	TD2
16	CD3	SA4	AP4	TD1

**Table 3.** Structural parameters of storage chamber.

Parameters (mm)	Value
Length of storage chamber	1,113
External diameter of storage chamber	108
Internal diameter of storage chamber	67
Thickness of aerogel insulation blanket	11.5
Length of aerogel insulation blanket	800
Effective storage volume	2.82

## 2.4 Experimental procedures

First, the storage chamber was pre-cooled with 2 L of liquid nitrogen for 5 min to reduce energy loss when the coolant was packed. The dry ice and alcohol contents were then measured and placed in an insulated pail. Liquid nitrogen was added to bring the mixture to the desired temperature, while stirring was continued to prevent solidification. After pre-cooling, the coolant was quickly pumped into the storage chamber, and the top lid was immediately attached. The storage chamber pressure was adjusted in advance based on the experimental requirements. Both the temperature and pressure sensors were calibrated in advance. The ambient temperature was approximately 293.15 K. In the previous sampling process, the average time for the hybrid pressure coring system was 86 min (Inada and Yamamoto, 2015). Therefore, the experiments were conducted for 120 min.

## 2.5 Energy efficiency and exergy calculation

### 2.5.1 Energy efficiency

Under exhaust conditions, coolant storage can be considered a steady-state process. Therefore, the experimental setup was considered as a multicylinder cylindrical wall heat transfer model, with subscripts 1, 2, 3 and 4 representing the storage chamber, inner stainless steel cylinder, insulation layer and outer stainless steel cylinder respectively.

The energy lost during the storage process  $Q_1$  (kJ) is:

$$Q_1 = \Phi T \quad (1)$$

$$\Phi = \frac{2\pi l(t_1 - t_4)}{\frac{1}{\lambda_1} \ln \frac{r_2}{r_1} + \frac{1}{\lambda_2} \ln \frac{r_3}{r_2} + \frac{1}{\lambda_3} \ln \frac{r_4}{r_3}} \quad (2)$$

where  $\Phi$  is the heat flow in W;  $T$  is the storage time in s;  $l$  is the length of the storage chamber in m;  $t$  is the temperature in K;  $\lambda$  is the coefficient of thermal conductivity in W/(m·K);  $r$  is the radius in m.

Then, the storage efficiency  $\eta$  (%) is:

$$\eta = 1 - \frac{|Q_1|}{m_i \gamma} \quad (3)$$

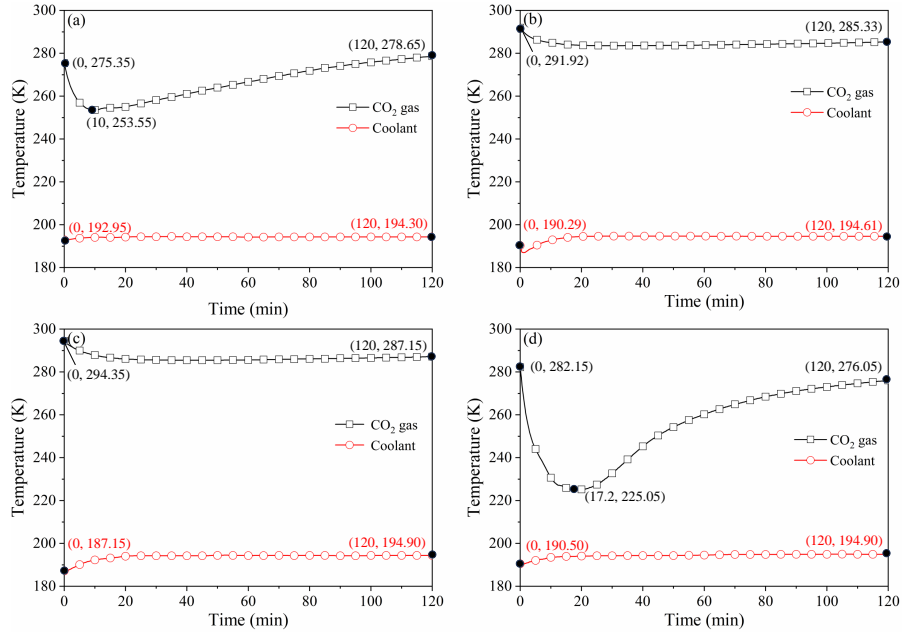


**Fig. 5.** Temperature change of coolant under atmospheric pressure conditions: (a) No. 1, (b) No. 5, (c) No. 9, and (d) No. 13.

where  $m_i$  is the mass of dry ice as 2.5 kg;  $\gamma$  is the latent heat of dry ice as 636 kJ/kg.

Under the condition of non-exhaust, the storage efficiency  $\eta$  (%) is:

$$\eta = \frac{Q_3 - Q_2}{Q_3} \quad (4)$$

$$Q_2 = Cm \Delta T_1 \quad (5)$$

$$Q_3 = Cm \Delta T_2 \quad (6)$$

where  $Q_2$  is the energy lost due to the increase in coolant temperature in kJ;  $Q_3$  is the energy carried by the coolant in kJ;  $C$  is the specific heat capacity of the coolant as 2,300 J/(kg·K);  $m$  is the mass of coolant is kg;  $\Delta T_1$  is the difference between the initial temperature and the final temperature of the coolant in K;  $\Delta T_2$  is the difference between the initial temperature of the coolant and the ambient temperature in K.

### 2.5.2 Exergy

The total physical exergy  $e$  (kJ/kg) of the coolant is:

$$e = e_p + e_s + e_l \quad (7)$$

The pressure exergy  $e_p$  (kJ/kg) generated by the pressure difference is:

$$e_p = zR(T_0) \ln \frac{P_s}{P_0} \quad (8)$$

where  $z$  is the amount of substance of gas in mol;  $R$  is the molar gas constant as  $8.31441 \pm 0.00026$  J/(mol·K);  $T_0$  is the temperature of the coolant after the experiment in K;  $P_0$  is the internal pressure of the storage chamber after the experiment in MPa;  $P_s$  is the initial pressure of the storage chamber as 0.1 MPa.

The sensible heat exergy  $e_s$  (kJ/kg) caused by temperature

difference is:

$$e_s = -c_p(T_0 - T_s) + c_p(T_0) \ln \frac{T_0}{T_s} \quad (9)$$

where  $c_p$  is the constant pressure heat capacity of the coolant as 2,300 J/(kg·K);  $T_s$  is the initial temperature of the coolant in K.

The latent heat exergy  $e_l$  (kJ/kg) caused by the phase change of dry ice is:

$$e_l = \left( \frac{T_0}{T_1} - 1 \right) \gamma \quad (10)$$

where  $T_1$  is the saturation temperature of the coolant in K.

## 3. Experimental results

### 3.1 Coolant temperature change under atmospheric pressure conditions

The coolant temperature was represented by the average of the three monitoring points, which was taken into account in all cases in this study. In addition, the dry ice and alcohol in the coolant would gradually stratify due to gravity. First, the changes in the coolant temperature under atmospheric pressure conditions were compared, as shown in Fig. 5. The changes are generally consistent, with the temperature peaking between 10 and 15 min and then remaining stable. It should be noted that the final temperatures of all four experiments were around 194.65 K, which was close to the critical pressure of dry ice at 0.1 MPa, regardless of the formula parameters. The temperature change of the gas followed a similar pattern, decreasing and then increasing, but at different rates, and the turning point was close to the moment when the coolant temperature reached a steady state. In the initial stage, while the coolant is still mixed, some of the dry ice produces low-temperature CO<sub>2</sub> by exchanging heat with the environment,

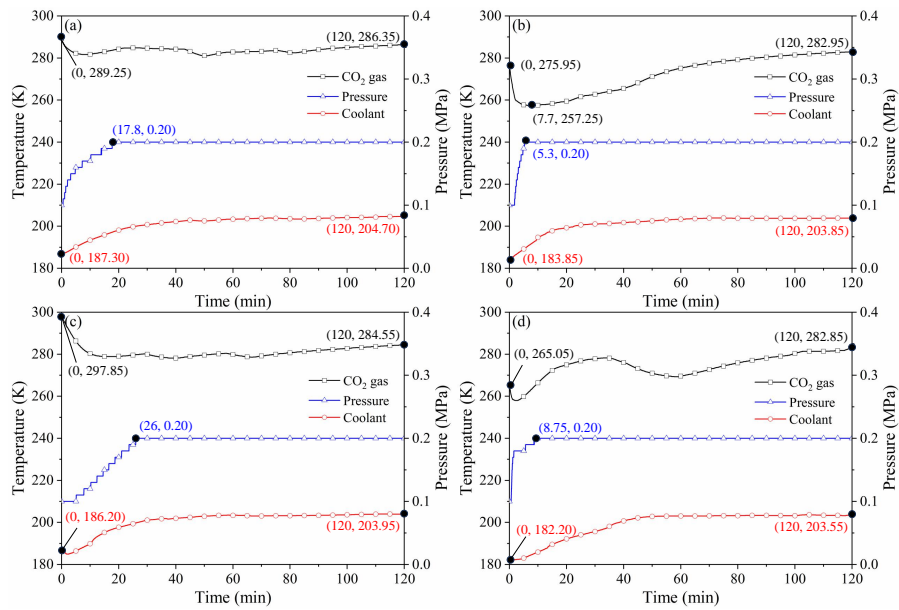


**Fig. 6.** Temperature change of coolant under 0.2 MPa pressure conditions: (a) No. 2, (b) No. 6, (c) No. 10, and (d) No.14.

resulting in some of the energy consumption. As the dry ice and alcohol stratified, the separating effect of the aerogel insulation blanket and low-temperature alcohol reduced the energy exchange between the dry ice and the environment and reduced the rate of heat transfer. However, the low-temperature CO<sub>2</sub> gas could still exchange heat with the surrounding gas, causing the temperature gradually rise.

### 3.2 Coolant temperature change under 0.2 MPa pressure conditions

The change in coolant temperature under 0.2 MPa pressure conditions was compared, as shown in Fig. 6. During the initial storage stage, the sublimation of dry ice in the coolant caused the gas temperature to decrease rapidly, while the coolant temperature increased gradually. However, the backpressure prevented CO<sub>2</sub> from being released in time, and the rising internal pressure led to a gradual increase in the critical gasification temperature of dry ice, which accelerated phase change. Consequently, throughout the early stages of the experiment, the coolant temperature increased during while the gas temperature fluctuated. Although No. 6 showed a slower rise in gas temperature, it was assumed to be for the same reason. The sublimation temperature of dry ice at 0.2 MPa was about 198 K. The final temperatures of the coolant in all the tests were higher than this value, indicating that the dry ice was always sublimable.

In addition, we also found that No. 6 and No. 14 pressures reached 0.2 MPa much earlier than the other tests. This may be due to the fact that the powder dry ice forms a compact solid layer under pressure, preventing further sublimation of the dry ice inside. Whereas No. 6 and No. 14 contained higher amounts of granular dry ice, which may have increased the effective heat transfer area. The dry ice could sublimate quickly, resulting in a rapid increase in temperature.

### 3.3 Coolant temperature change under 0.4 MPa pressure conditions

The change in coolant temperature at 0.4 MPa pressure conditions was compared, as shown in Fig. 7. The temperature changes in the gas and coolant were similar to that of 0.2 MPa. The coolant temperature was steadily increased until the pressure rose to 0.4 MPa. More granular dry ice did not increase pressure as quickly which could be attributed to the higher critical sublimation temperature of the dry ice. The sublimation temperature of dry ice (0.4 MPa) is approximately 204 K, which significantly inhibits sublimation.

### 3.4 Coolant temperature change under non-exhaust conditions

The changes in coolant temperature under non-exhaust conditions were compared, as shown in Fig. 8. As dry ice continuously sublimated to CO<sub>2</sub>, the AP increased rapidly, and the time to reach 0.52 MPa, which is the triple point of dry ice were nearly identical. The rate of AP increase was dependent on the sublimation rate of dry ice, but the effects of the other factors did not appear to have a noticeable difference. At this stage, dry ice is more likely to melt than sublimate, therefore the rate of increase in gas and coolant temperatures begin to slow. However, this contradicted with the experimental observation that there was no further increase in AP when the dry ice melted. The following processes could occur in the storage chamber. At 0.52 MPa, the surface dry ice stopped sublimating. However, the surface dry-ice layer had a protective effect, and the AP could not be applied instantly to the internal dry ice. Heat transfer causes the top dry ice to melt, while the inside dry ice may have a transitory sublimation response, followed by the release of CO<sub>2</sub>. The AP increase, as seen in No. 4. This circulated continuously in the storage chamber. As the AP increased, the experimental conditions

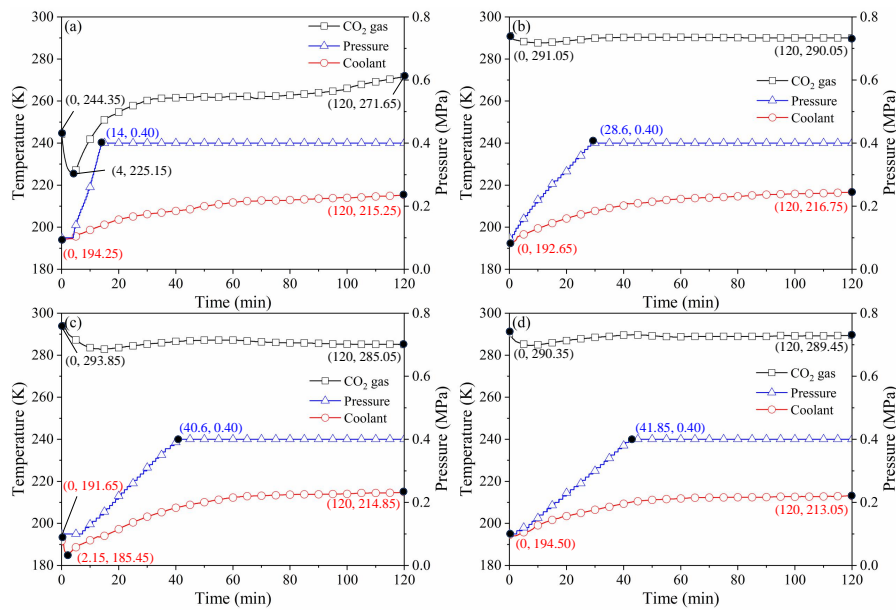


**Fig. 7.** Temperature change of coolant under 0.4 MPa pressure conditions: (a) No. 3, (b) No. 7, (c) No. 11, and (d) No. 15.

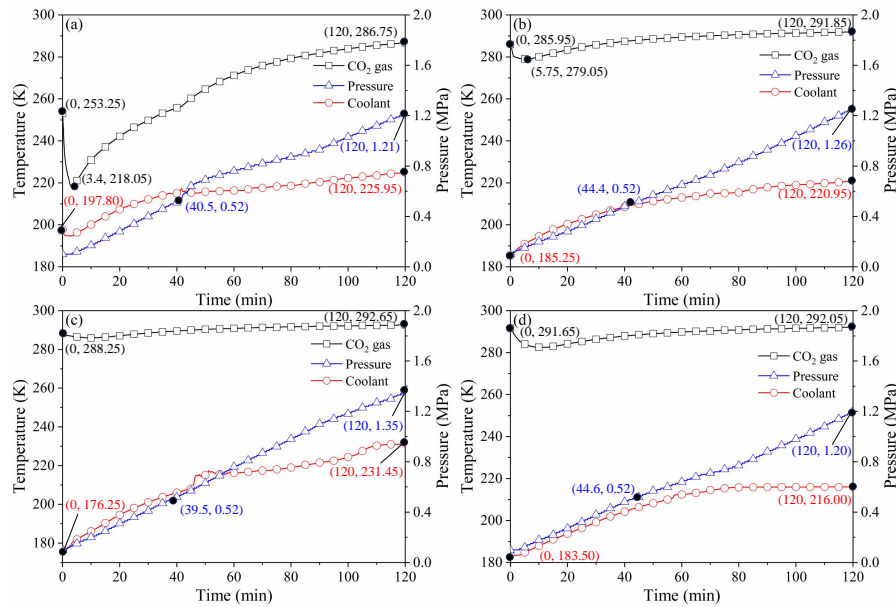


**Fig. 8.** Temperature change of coolant under non-exhaust conditions: (a) No. 4, (b) No. 8, (c) No. 12, and (d) No. 16.

shifted from the solid-liquid phase equilibrium line, making sublimation more difficult. The coolant temperature steadily stabilized, as observed in No. 16.

## 4. Analysis of energy utilization

### 4.1 Storage efficiency

The storage performance of the coolant was evaluated based on its storage efficiency, and the results are presented in Fig. 9. When CO<sub>2</sub> gas could not be released, the storage efficiency was only 61.8%-67.13%, which was much lower than the other test groups, regardless of other factors. Under conditions where CO<sub>2</sub> could be released, dry ice sublimation

would absorb a large amount of heat, slowing the rate of increase in coolant temperature and effectively improving the storage efficiency. However, when CO<sub>2</sub> was not released in time, the AP increased to a triple point. As shown in the above analysis, the surface dry ice melted before the sublimation of the internal dry ice. As the heat absorbed through sublimation was higher than absorbed through melting, the loss of dry ice increased. As the AP increased further, an increasing amount of dry ice melted; thus, the storage efficiency decreased significantly. It is clear that the AP is a significant factor affecting the storage efficiency.

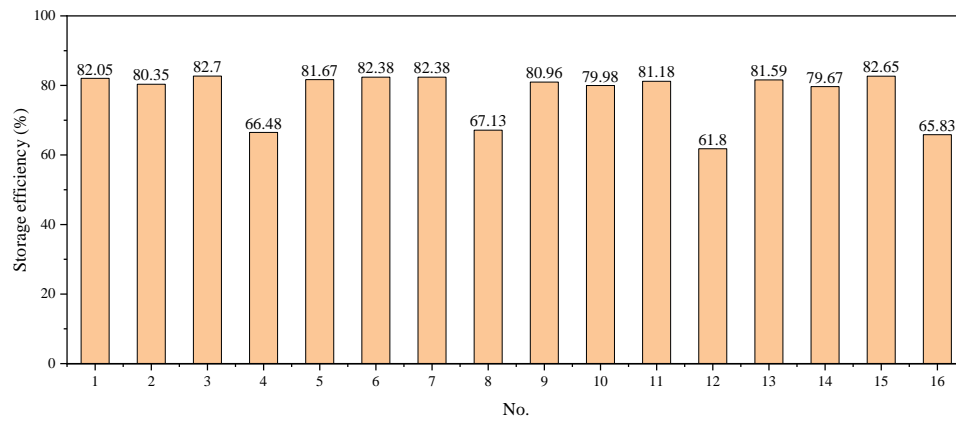


**Fig. 9.** Storage efficiency of coolant under different conditions.

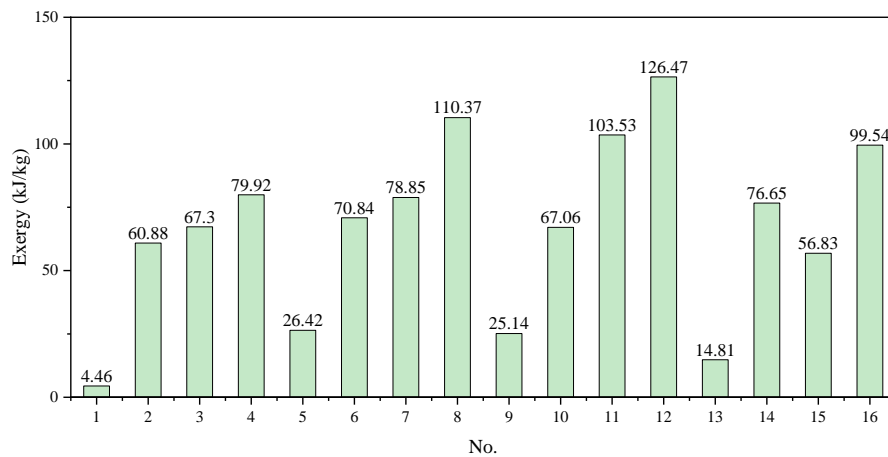


**Fig. 10.** Exergy of coolant under different conditions.

## 4.2 Exergy

The calculated exergy results are presented in Fig. 10. Note that the exergy consumed during storage is used to exchange energy with the environment; this process is irreversible. The consumed exergy was not available for freezing the hydrate cores. Therefore, the results calculated using Eqs. (7)-(10) are defined as the exergy loss. In the tests in which all gases were freely released, the exergy loss was significantly lower than that of the others. The freeze-sampling technique primarily utilizes the phase-change properties of dry ice. The SA, TD, and CD primarily affect the heat-transfer rate, whereas the AP interferes with the phase-change path of dry ice. Once the dry ice cannot sublimate to CO<sub>2</sub> quickly but melts instead, an irreversible loss of latent heat occurs, preventing the hydrate cores from freezing quickly to the predetermined temperature, resulting in sampling failures. Therefore, AP must be considered as the primary factor in the principles of the freeze-sampling technique. To ensure proper sampling, CO<sub>2</sub> must be released in a timely manner to maintain a stable AP in the storage chamber.

## 4.3 Range analysis

Further range analysis was performed to obtain clear guidance for parameter optimization of the coolant combination, as shown in Fig. 11. The R-value represents the degree to which certain factors influence one another. As can be seen, the AP has a significant impact on the storage efficiency and exergy, mainly by changing the phase-change path. Increased AP could result in an increase in the critical sublimation temperature of dry ice, resulting in dry ice loss. Simultaneously, as it is close to the triple point, the possibility of dry ice melting can cause latent heat loss. The SA had a reduced effect on heat transfer rate. Granular dry ice has a small SA and can significantly enhance storage efficiency. However, powder dry ice does not appear to have the expected low storage efficiency, which could be attributed to its ability to form a compact dry ice layer that provides effective protection for internal dry ice. In terms of exergy, it is reasonable to expect that SA would cause significant sublimation and melting of dry ice, resulting in exergy loss. The CD primarily affects coolant volume. Although low-temperature alcohol may partition following stratification, increasing coolant volume promotes heat exchange between the low-temperature alcohol and the surroundings. The TD has the least influence on the

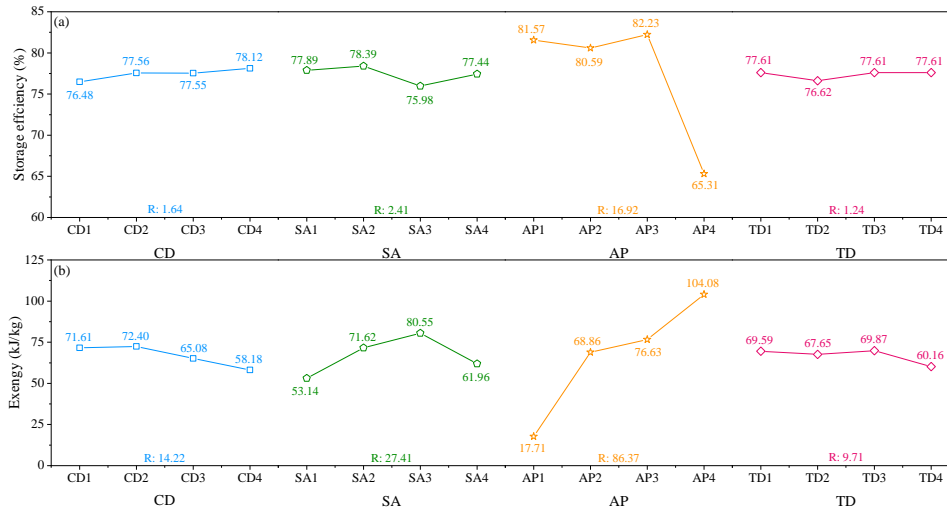


**Fig. 11.** Range analysis for the effect of different factors on: (a) storage efficiency and (b) exergy.

heat transfer rate. A lower TD efficiently controlled CO<sub>2</sub> generation and also reduced the effect of AP on dry ice phase shift.

#### 4.4 Correlation analysis

The relationship between each factor, storage efficiency, and exergy was investigated using Pearson's correlation analysis. The correlation results show that the correlation coefficients of CD, SA and TD with storage efficiency and exergy are all close to 0 and the p-value is much higher than 0.05, indicating that there is no significant correlation. However, the correlation coefficient between AP and storage efficiency was -0.740, with a significant p-value at the 0.01 level, indicating a negative correlation. At the same time, the correlation coefficient between the AP and exergy was 0.880, and the p-value was significance at the 0.01 level, indicating a positive correlation. The results show that AP has a decisive role in the coolant storage process, while CD, SA and TD need to be comprehensively analyzed combined with the coolant injection process.

#### 4.5 Analysis of the coolant storage mechanism

Based on the above analysis, Fig. 12 depicts a hypothetical storage mechanism for natural gas hydrates during the coolant storage phase of the hole-bottom freeze-sampling technique. When the sampler was lowered, low-temperature alcohol and dry ice separated due to gravity. The external environment exchanges heat with the alcohol layer, which causes dry ice to sublimate and generates CO<sub>2</sub> and AP in the storage chamber. AP affects the phase-change process of dry ice. Once the AP in the storage chamber exceeds the triple point, the dry ice begins to melt, resulting in a significant loss of latent heat, which is a major factor affecting coolant storage. TD, CD, and SA play supportive roles in this process. SA had an unexpected consequence. The powder dry ice is denser in the created solid layer and provides significant interior protection rather than impending dry ice sublimation or melting. However, granular

dry ice diminishes this effect and promotes dry ice sublimation in conjunction with high TD and low CD under conditions conducive to gas depletion. This results in a rapid reduction in coolant temperature allowing the storage efficiency to be effectively regulated at approximately 80%. However, this results in high consumption of dry ice, increasing exergy. This also promotes dry ice melting where exhaust is not allowed. However, because sublimation absorbs more heat than melting, dry ice loses a large amount of latent heat, resulting in a fall in storage efficiency and an increase in exergy. Therefore, when considering the storage capacity of the coolant in the hole-bottom freeze-sampling technique for natural gas hydrate, AP needs to be given critical attention, while other factors need to be considered in the overall sampling process.

In summary, for 2.5 kg of dry ice, the alcohol content of the coolant should be 1.0 L. The initial TD between the coolant and environment was 105 K, and the AP was 0.1 MPa. However, the SA was 1:1 for powder, granular, and completely powder. In our previous work, the overall selection of granular dry ice was considered reasonable (Guo et al., 2021), which could help minimize energy loss during coolant injection. Coolant storage is intended to conserve sufficient cold energy during the sampler-lowering process; nonetheless, the ultimate goal is to ensure the success of the freeze-sampling technique. Therefore, according to the experimental results and considering the minimization of the energy loss caused by viscosity and heat transfer rate during the injection process, it is still reasonable to completely use granular dry ice. The storage efficiency was 77.44% and the exergy loss was 61.96 kJ/kg, which is reasonable.

#### 5. Conclusion

In this study, the key factors affecting the storage capacity of the coolant during the freezing sampling process of natural gas hydrate are investigated, and the optimized formulation is obtained based on this. The following conclusions can be drawn:

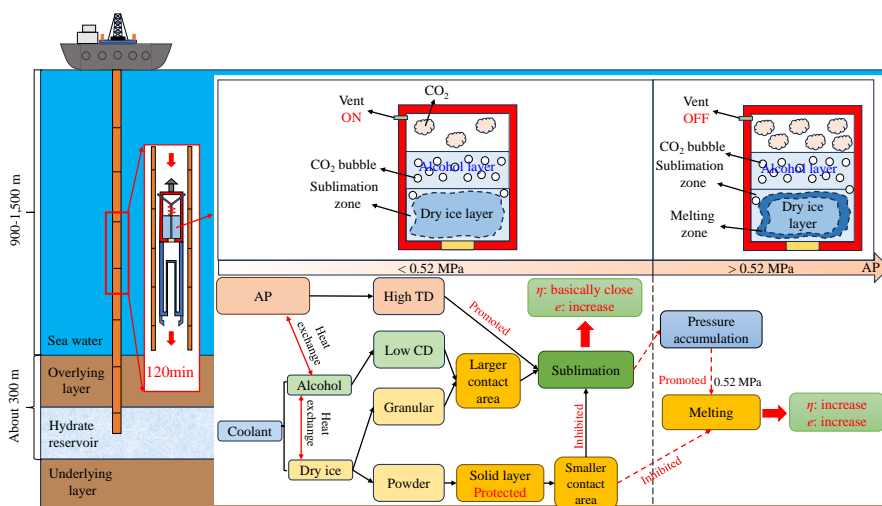


**Fig. 12.** Coolant storage mechanism.

- 1) Pressure is the primary factor impacting coolant storage capacity, altering the dry ice phase-change path and resulting in latent heat loss. The timely release of CO<sub>2</sub> from the storage chamber can effectively ensure the success of freezing sampling.
- 2) Considering the negative effects of the viscosity and heat transfer area of the coolant during injection, dry ice with a low specific surface area may be more useful for application.
- 3) Excessive alcohol consumption accelerates the rate of heat exchange with the environment, leading to energy loss.
- 4) The temperature difference between the coolant and environment should not be excessive. High-temperature coolants are more storable because they provide enough cold energy.
- 5) In summary, the optimized formula is as follows. The coolant is blended with granular dry ice and 1 L of alcohol, and the difference between its initial and ambient temperatures should be maintained at 105 K with a working pressure of 0.1 MPa.

### Acknowledgements

This work was supported by the National Natural Science Foundation of China (Nos. 42102347, 51991364, and 51890914), the Young and Middle-aged Excellent Team Project for Scientific and Technological Innovation of Jilin Province of China (No. 20220508135RC), the Program for JLU Science and Technology Innovative Research Team (No. 2020TD-05), and the Fundamental Research Funds for the Central Universities.

### Conflict of interest

The authors declare no competing interest.

**Open Access** This article is distributed under the terms and conditions of the Creative Commons Attribution (CC BY-NC-ND) license, which permits unrestricted use, distribution, and reproduction in any medium, provided the original work is properly cited.

### References

Ali, M., Jha, N. K., Pal, N., et al. Recent advances in carbon dioxide geological storage, experimental procedures, influencing parameters, and future outlook. *Earth-Science Reviews*, 2022, 225: 103895.

Babakhani, S. M., Bahmani, M., Shariati, J., et al. Comparing the capability of artificial neural network (ANN) and CSMHYD program for predicting of hydrate formation pressure in binary mixtures. *Journal of Petroleum Science and Engineering*, 2015, 136: 78-87.

Falenty, A., Kuhs, W. F., Glockzin, M., et al. "Self-preservation" of CH<sub>4</sub> hydrates for gas transport technology: Pressure-temperature dependence and ice microstructures. *Energy & Fuels*, 2014, 28(10): 6275-6283.

Gudmundsson, J. S., Parlaktuna, M., Khokhar, A. A. Storage of natural gas as frozen hydrate. *SPE Production & Facilities*, 1994, 9(1): 69-73.

Guo, J., Chen, J., Ren, Z., et al. Pressure-retaining sampler for sediment and overlying seawater based on heavy duty ROV-Jellyfish. *Deep Sea Research Part I: Oceanographic Research Papers*, 2023, 196: 104007.

Guo, W., Lei, J., Zhang, P., et al. Optimisation of freezing efficiency of hole-bottom freezing technique for gas hydrate sampling: Study on factors influencing dry ice phase transition. *Journal of Natural Gas Science and Engineering*, 2021, 85: 103705.

Guo, W., Zhang, P., Yang, X., et al. Development and application of hole-bottom freezing drilling tool for gas-hydrate-bearing sediment sampling. *Ocean Engineering*, 2020, 203: 107195.

Inada, N., Yamamoto, K. Data report: Hybrid pressure coring system tool review and summary of recovery result from gas-hydrate related coring in the Nankai project. *Marine and Petroleum Geology*, 2015, 66: 323-345.

Jansen, S., Woudstra, N. Understanding the exergy of cold: Theory and practical examples. *International Journal of Exergy*, 2010, 7(6): 693-713.

- Kang, Z., Zhao, Y., Yang, D. Review of oil shale in-situ conversion technology. *Applied Energy*, 2020, 269: 115121.
- Kong, Z., Jiang, Q., Dong, X., et al. Estimation of China's production efficiency of natural gas hydrates in the South China Sea. *Journal of Cleaner Production*, 2018, 203: 1-12.
- Kumar, P., Collett, T.S., Boswell, R., et al. Geologic implications of gas hydrates in the offshore of India: Krishna-Godavari basin, Mahanadi basin, Andaman Sea, Kerala-Konkan basin. *Marine and Petroleum Geology*, 2014, 58: 29-98.
- Li, J., Ye, J., Qin, X., et al. The first offshore natural gas hydrate production test in South China Sea. *China Geology*, 2018, 1(1): 5-16.
- Lu, C., Xia, Y., Sun, X., et al. Permeability evolution at various pressure gradients in natural gas hydrate reservoir at the Shenhu Area in the South China Sea. *Energies*, 2019, 12(19): 3688.
- Middleton, R. S., Gupta, R., Hyman, J. D., et al. The shale gas revolution: Barriers, sustainability, and emerging opportunities. *Applied energy*, 2017, 199: 88-95.
- Riedel, M., Collett, T., Malone, M. Expedition 311 synthesis: Scientific findings. *International Ocean Discovery Program Publications*, 2010, 311.
- Ryu, B. J., Collett, T. S., Riedel, M., et al. Scientific results of the second gas hydrate drilling expedition in the Ulleung basin (UBGH2). *Marine and Petroleum Geology*, 2013, 47: 1-20.
- Schultheiss, P., Holland, M., Humphrey, G. Wireline coring and analysis under pressure: Recent use and future developments of the HYACINTH system. *Scientific Drilling*, 2009, 7: 44-50.
- Sloan Jr, E. D., Koh, C. A., Koh, C. A. *Clathrate Hydrates of Natural Gases*. Boca Raton, USA, CRC Press, 2007.
- Stern, L. A., Circone, S., Kirby, S. H. et al. Anomalous preservation of pure methane hydrate at 1 atm. *The Journal of Physical Chemistry B*, 2001, 105(9): 1756-1762.
- Stern, L. A., Lorenson, T. D. Grain-scale imaging and compositional characterization of cryo-preserved India NGHP 01 gas-hydrate-bearing cores. *Marine and Petroleum Geology*, 2014, 58: 206-222.
- Sun, Y., Wang, Y., Guo, W. et al. Hole-bottom freezing technique based on phase change heat transfer for gas-hydrates sampling: Efficiency optimization of refrigeration change of phase. *Applied Thermal Engineering*, 2018, 130: 722-734.
- Sun, Y., Wang, Y., Lü, X., et al. Hole-bottom freezing method for gas hydrate sampling. *Journal of Natural Gas Science and Engineering*, 2015, 25: 271-283.
- Tsuji, H., Kobayashi, T., Okano, Y., et al. Thermodynamic simulations of isobaric hydrate-forming operations: Formulation of computational scheme and its application to hydrate formation from a methane + ethane + propane mixture. *Energy & Fuels*, 2005, 19(4): 1587-1597.
- Wang, H., Li, Y., Huang, L., et al. A pore-scale study on microstructure and permeability evolution of hydrate-bearing sediment during dissociation by depressurization. *Fuel*, 2024, 358: 130124.
- Wang, J., Yu, M., Qian, D., et al. Optimisation of drainage performance of the thin-walled core barrel sealing technology for pressure preservation sampling. *Ocean Engineering*, 2022, 250: 110996.
- Wang, Y., Xu, T., Zhang, P., et al. Experimental investigation of coolant selection and energy efficiency analysis during gas hydrate-bearing sediment freeze-sampling. *International Journal of Refrigeration*, 2020, 120: 221-236.
- Xia, Y., Xu, S., Lu, C., et al. Characterization and capillary pressure curve estimation of clayey-silt sediment in gas hydrate reservoirs of the South China Sea. *Advances in Geo-Energy Research*, 2023, 10(3): 200-207.
- Xiao, K., Zou, C., Yang, Y., et al. A preliminary study of the gas hydrate stability zone in a gas hydrate potential region of China. *Energy Science & Engineering*, 2020, 8(4): 1080-1091.
- Xue, Y., Liu, J., Liang, X., et al. Ecological risk assessment of soil and water loss by thermal enhanced methane recovery: Numerical study using two-phase flow simulation. *Journal of Cleaner Production*, 2022, 334: 130183.
- Yamamoto, K., Inada, N., Kubo, S., et al. A pressure coring operation and on-board analyses of methane hydrate-bearing samples. Paper OTC 25305 Presented at Offshore Technology Conference, Houston, Texas, 5-8 May, 2014.
- Ye, J., Qin, X., Xie, W., et al. The second natural gas hydrate production test in the South China Sea. *China Geology*, 2020, 3(2): 197-209.
- Zhang, L., Dong, H., Dai, S., et al. Effects of depressurization on gas production and water performance from excess-gas and excess-water methane hydrate accumulations. *Chemical Engineering Journal*, 2022a, 431: 133223.
- Zhang, P., Wang, Y., Jia, R., et al. Dissociation characteristic of methane hydrate in clayey silt below the ice point. *Journal of Natural Gas Science and Engineering*, 2022b, 100: 104443.
- Zhang, X., Zhang, S., Yuan, Q., et al. Gas production from hydrates by CH<sub>4</sub>-CO<sub>2</sub> replacement: Effect of N<sub>2</sub> and intermittent heating. *Energy*, 2024, 288: 129965.
- Zhao, L., Mao, W., Liu, Z., et al. Research on the differential tectonic-thermal evolution of Longmaxi shale in the southern Sichuan Basin. *Advances in Geo-Energy Research*, 2023, 7(3): 152-163.
- Zhu, L., Wu, S., Zhou, X., et al. Saturation evaluation for fine-grained sediments. *Geoscience Frontiers*, 2023, 14(4): 101540.
- Zou, Q., Chen, Z., Cheng, Z., et al. Evaluation and intelligent deployment of coal and coalbed methane coupling coordinated exploitation based on Bayesian network and cuckoo search. *International Journal of Mining Science and Technology*, 2022, 32(6): 1315-1328.